Research Article | Vol. 13, No. 4 / 1 Apr 2022 / Biomedical Optics Express 2450
Biomedical Optics EXPRESS

Optimization of photo-biomodulation therapy for wound healing of diabetic foot ulcers *in vitro* and *in vivo*

QIANQIAN CHEN,[1,2,5] JICHUN YANG,[1,5] HUIJUAN YIN,[1,*] YINGXIN LI,[1] HAIXIA QIU,[3] YING GU,[3] HUA YANG,[4] DONG XIAOXI,[1] SHI XIAFEI,[1] BOCHEN CHE,[1] AND HONGXIAO LI[1]

[1]*Laboratory of Laser Medicine, Institute of Biomedical Engineering, Chinese Academy of Medical Sciences, Peking Union Medical College, Tianjin 300192, China*
[2]*National Research Center for Rehabilitation Technical Aids, Beijing Key Laboratory of Rehabilitation Technical Aids for Old-Age Disability, Key Laboratory of Human Motion Analysis and Rehabilitation Technology of the Ministry of Civil Affairs, Beijing 100176, China*
[3]*Department of Laser Medicine, Chinese PLA General Hospital, Beijing 100853, China*
[4]*Semiconductor Lighting Technology Research and Development Center, Institute of Semiconductors, Chinese Academy of Sciences, Beijing 100083, China*
[5]*Equal contributors*
[*]*yinhj@bme.pumc.edu.cn*

Abstract: Unclear optical parameters make photo-biomodulation (PBM) difficult to implement in diabetic foot ulcer (DFU) clinically. Here, 12 wavelengths (400–900 nm) were used to conduct PBM to heal DFU wounds in vitro and in vivo. PBM at 10 mW/cm^2 and 0.5–4 J/cm^2 with all 12 wavelengths promoted proliferation of diabetic wound cells. In a mimic DFU (mDFU) rat model, PBM (425, 630, 730, and 850 nm, and a combination light strategy) promoted mDFU healing. The positive cell proliferation, re-epithelialization, angiogenesis, collagen synthesis, and inflammation were possible mechanisms. The combination strategy had the best effect, which can be applied clinically.

1. Introduction

Diabetes mellitus (DM) can cause serious complications in many tissues and organs. Diabetic foot ulcers (DFUs) are a common complication. DFU patients can have non-healing or long-lasting chronic skin ulcers with the risk of amputation, high costs, and reduced quality of life and lifespan. Treatment mainly includes blood glucose control, anti-infection drugs, and wound bed preparation and debridement [1,2]. However, the effects are not ideal and the 5-year mortality rate after amputation remains high [3].

Photo-biomodulation (PBM) was previously referred to as low-level laser therapy (LLLT). It is a non-invasive, painless treatment with few side-effects and may be an option to treat DFUs. Many studies have confirmed the positive healing effect of PBM on diabetic wounds [4–6]. However, the application of wavelengths and light doses in different studies is not uniform; thus, the best protocol for PBM of DFUs has been debated [7,8]. Although most studies agree that 4–10 J/cm^2 is the optimal dose for proliferation [9,10], studies using other irradiation parameters have also presented beneficial effects [11,12]. A biphasic response in terms of the Arndt–Schulz rule has also been demonstrated several times when using PBM [8]. PBM implements beneficial and destructive effects with changes in optical parameters and doses [13,14]. Therefore, optimization of irradiation parameters has always been a core issue in the clinical application of PBM.

The therapeutic mechanism of PBM is unclear. It is generally believed that a photochemical reaction occurs after absorption of a photon by a chromophore in the cell, that is, the photoreceptor

#451135 https://doi.org/10.1364/BOE.451135
Journal © 2022 Received 7 Jan 2022; revised 15 Mar 2022; accepted 17 Mar 2022; published 25 Mar 2022

Biomedical Optics EXPRESS

of PBM. Cytochrome c oxidase (CCO) is the main chromophore that absorbs red and near-infrared (NIR) light [15–18]. Light-gated ion channels and channel rhodopsin are chromophores activated by green and blue light [18]. Wound healing is a complex event divided into various and overlapping phases, including inflammation, proliferation, and remodeling phases. These processes require the participation of various cells including keratinocytes, macrophages and myofibroblasts. Angiogenesis and the formation of extracellular matrix, such as collagen deposition, also participate in wound healing [19–21]. We believe that PBM wavelength studies should not focus solely on red/infrared light corresponding to CCO and should also not ignore the blue–green light corresponding to other photoreceptors.

In this study, a wide-spectrum range of light-emitting diodes (LEDs) (400–900 nm) was thus used to conduct PBM in in vitro and in vivo DFU models. We attempted to identify an optimal strategy for PBM treatment of DFUs and explain the possible mechanism of action using a large amount of data.

2. Materials and methods

2.1. Materials

Human immortalized keratinocytes (HaCaT) and the human monocyte-like cell line U937 were obtained from the National Infrastructure of Cell Line Resource (Beijing, China). Human skin fibroblasts (WS1) and human umbilical vein endothelial cells (HUVECs) were purchased from the ATCC (VA, USA). CD (SD) IGS rats were purchased from Charles River Laboratories (Beijing, China). RPMI-1640, fetal bovine serum (FBS), antibiotic-antimycotic, sodium pyruvate, non-essential amino acids (NEAAs), and L-glutamine were obtained from Gibco-Life Technologies (Gaithersburg, MD, USA). Modified Eagle's Medium (MEM) with Earle's Balanced Salt Solution (EBSS) was purchased from Hyclone (Logan, UT, USA). Endothelial Cell Growth Medium (EGM)-2 Bullet Kit was obtained from Lonza (Walkersville, MD, USA). D-glucose, streptozocin (STZ), and all other chemicals were obtained from Sigma-Aldrich (Munich, Germany). The high-fat diet was from Beijing China Fu Kang Biological Technology Co., Ltd. (Beijing, China). The adenosine triphosphate (ATP) assay kit, bicinchoninic acid (BCA) Protein Assay Kit, enzyme-linked immunosorbent assay (ELISA) kit, and Masson's Trichrome Stain Kit were purchased from Beyotime (Shanghai, China). Monoclonal antibodies against proliferating cell nuclear antigen (PCNA), CD34, CD11B, and matrix metalloproteinase (MMP)-9 were purchased from Abcam (Cambridge, UK).

2.2. LED devices

LED devices are shown in Fig. 1 and were made by Semiconductor Lighting Technology Research and Development Center, Institute of Semiconductors, Chinese Academy of Sciences (CAS) (Beijing, China) (Fig. 1(a) and 1 (b)) and the Laboratory of Laser Medicine, Institute of Biomedical Engineering, Chinese Academy of Medical Sciences & Peking Union Medical College (Tianjin, China) (Fig. 1(c)–1(h)).

2.3. Cell culture

Briefly, HaCaT and WS1 cells were cultured in MEM-EBSS complete medium containing 10% (v/v) FBS, 1 mM sodium pyruvate, 1% antibiotic-antimycotic, and 0.1 mM NEAAs. HUVECs were cultured in EGM-2 Bullet Kit. U937 monocytic cells were induced to differentiate into macrophage-like cells by treatment with 20 ng/mL phorbol 12-myristate 13-acetate synthetic (Sigma-Aldrich) and cultured in RPMI-1640 medium supplemented with 10% (v/v) FBS. Cells were incubated in a humidified atmosphere at 37°C with 5% CO_2.

Biomedical Optics EXPRESS

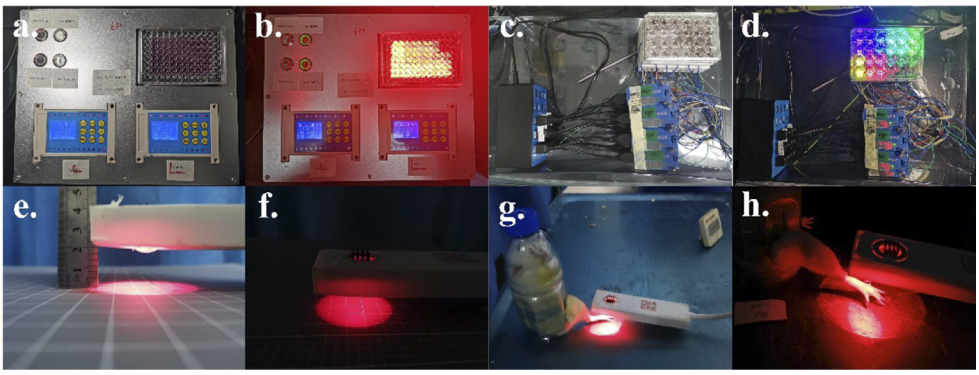

Fig. 1. LED devices. (a, b) LED devices for 96-well plates (405, 425, 455, 495, 510, 530, 560, 630, 660, 730, 805, and 850 nm). Four LED beads as one irradiation unit, corresponding to four wells, with an output ranging from 10 to 40 mw/cm^2 light. The irradiation time of each irradiation unit was controlled separately. (c, d) The LED array for the 24-well-plate output of 10 mw/cm^2 light integrated 12 wavelengths (405, 425, 455, 495, 510, 530, 560, 630, 660, 730, 805, and 850 nm). (e–h) LED devices (425, 510, 630, 730, and 850 nm) for rats with an output irradiance of 10 mW/cm^2 light at a distance of 2 cm and beam spot of 5 cm.

2.4. *In vitro diabetes models*

To examine the effect of high glucose on cells, HaCaT cells, HUVECs, WS1 cells, and U937 monocytic cells were exposed to 1, 2, 4, 6, 8, and 10 g/L D-glucose for 3 days. An MTT assay was used to evaluate cell proliferation.

2.5. *PBM therapy for cell proliferation in vitro*

Irradiation was performed with the set of LED devices shown in Fig. 1(a) and 1(b). Wavelengths were 405, 425, 455, 495, 510, 530, 560, 630, 660, 730, 805, and 850 nm. The irradiation parameters are listed in Table 1a. Irradiation was applied at powers of 10 and 40 mW/cm^2. The radiant exposures were 0.5, 1, 2, 4, 6, 8, and 10 J/cm^2. Cells were irradiated through the bottom of a 96-well plate. Cells in the control group were sham-irradiated. During the experiment, cells were protected from external light.

2.6. *MTT assay*

An MTT assay was used to assess the cell metabolism after PBM therapy for 24 h. The MTT assay is a colorimetric non-clonogenic assay that measures cell viability in culture by metabolic activity. Cell cultures were stained with a yellow tetrazolium substrate [3-(4, 5-dimethylthiazol-2-yl)-2, 5-diphenyltetrazolium bromide] (MTT; 5 mg/ml). Cells metabolized the substrate by reduction with nicotinamide adenine dinucleotide, producing purple, water insoluble, formazan crystals. A solvent (10% SDS and 50% DMF) was used to dissolve the crystals. A plate reader was used to measure the optical density (OD) at 570 nm. Absorbance values were indicative of the metabolic activity of surviving cells, which represented the cell count. The MTT assay was used for high-throughput analysis to measure the efficacy of PBM on cells.

2.7. *PBM therapy for cellular ATP metabolism, secretion, and migration in vitro*

Irradiation was performed with an LED device adapted to a 24-well plate as shown in Fig. 1(c) and 1(d). The irradiation parameters are listed in Table 1b, which were screened using MTT assay data.

Biomedical Optics EXPRESS

Table 1. PBM therapy parameters in vitro and in vivo

a. PBM therapy parameters for cell proliferation in vitro

Power density (mW/cm^2)	Time (s)	Energy density (J/cm^2)
0	0	0
10	50	0.5
10	100	1.0
10	200	2.0
10	400	4.0
10	600	6.0
10	800	8.0
10	1000	10.0
40	12.5	0.5
40	25	1.0
40	50	2.0
40	100	4.0
40	150	6.0
40	200	8.0
40	250	10.0

b. Grouping and PBM treatment parameters for cellular ATP metabolism, secretion, and migration in vitro

Cells	Power density (mW/cm^2)	Energy density (J/cm^2)
WS1	10	2
HACAT	10	0.5
HUVEC	10	0.5
U937	10	1

c. Grouping and protocols in vivo

GROUPS		PBM
Blank control group	C0	—
T2DM control group	CDM	—
PBM groups	PBM425	425 nm, 4J/cm^2
	PBM510	510 nm, 4J/cm^2
	PBM630	630 nm, 4J/cm^2
	PBM730	730 nm, 4J/cm^2
	PBM850	850 nm, 4J/cm^2
	PBMcom	Multi-wavelength Day 1-7 (inflammatory phase): 510 nm 2J/cm^2 and 850 nm 2J/cm^2 Day 7-11 (proliferation phase): 510 nm 2J/cm^2 and 630 nm 2J/cm^2 Day 11-21 (remodeling phase): 425 nm 2J/cm^2 and 730 nm 2J/cm^2

2.8. ATP measurement

The ATP level in cell lysates was determined using an ATP Bioluminescence Assay Kit (Beyotime, China) in accordance with the instructions. Briefly, 200 µl lysis buffer was added to each well of a 24-well plate, followed by centrifugation at 12,000 × *g* for 5 min at 4°C. The ATP level was determined by mixing 20 µl of the supernatant with 100 µl luciferase reagent, which catalyzed light production from ATP and luciferin. The emitted light was linearly related to the ATP concentration and measured using a microplate luminometer. The relative ATP level was calculated by the following formula: relative ATP level = ATP value/protein value.

Biomedical Optics EXPRESS

2.9. ELISAs

Commercially available ELISA kits (Beyotime) were used to measure interleukin (IL)-1β, IL-6, and intercellular adhesion molecule 1 (ICAM-1) concentrations in culture supernatants in accordance with the instructions. Briefly, culture supernatants were collected at 24 hours after PBM. The samples and standards were added and incubated for 2 hours. Biotinylated antibodies were added for detection. HRP-streptavidin and tetramethylbenzidine were added to develop color. The OD value was measured spectrophotometrically at 450 nm (Multiskan Spectrum; ThermoFisher, USA).

2.10. Migration assay

A scratch assay was performed in a 24-well plate to assess cell migration. A wound was made with a sterile 1-ml pipette tip and irradiated in accordance with section 2.7. An inverted microscope (CKX53; Olympus, Tokyo, Japan) connected to a CCD camera (HTC694ICE-1; Beijing, China) was used to capture images. Images were obtained again after 24 hours of incubation. Image J software (Rawak Software Inc., Stuttgart, Germany) was used to measure the scratched area. The migration rate (%) was reached as Eq. (1):

$$Migration\ rate\ (\%) = \frac{S_{\text{Wound area at 0h}} - S_{\text{Wound area at 12h}}}{S_{\text{Wound area at 0h}}} \times 100\% \quad (1)$$

2.11. Animals

Eighty male CD (SD) rats aged 6 weeks weighing between 180 and 200 g from Charles River Laboratories (Beijing, China) were used. Animals were kept at a controlled temperature (23 ± 2°C) in 12-h light/dark cycle with ad libitum access to food and water. This study was approved by the Animal Ethical and Welfare Committee at the Chinese Academy of Medical Sciences & Peking Union Medical College, Institute of Radiation Medicine (Approval No.: IRM-DWLL-2018124). All applicable institutional and/or national guidelines for the care and use of animals were followed.

2.12. Experimental groups

Animals were divided into three groups by simple randomization: (1) healthy rats not submitted to a high-fat diet or PBM (C0, n = 10); (2) type 2 diabetes mellitus (T2DM) rats without PBM therapy (CDM, n = 10); (3) T2DM rats with various PBM therapies, including PBM at 425 nm (n = 10), 510 nm (n = 10), 630 nm (n = 10), 730 nm (n = 10), 850 nm (n = 10), and multiple wavelength combinations (PBMcom, n = 10) (Fig. 2).

2.13. Experimental rat model of type 2 diabetes mellitus

CD (SD) rats were fed a high-fat diet (37.89% carbohydrate, 45.65% fat, and 16.46% protein [1042; Beijing China Fu Kang Biological Technology Co., Ltd., Beijing, China]) for 12 weeks. A low dose of STZ in citrate buffer (30 mg/kg, pH 4.5) was injected via the tail vein. The blood glucose concentration was measured after 1 week (day 0). If the blood glucose concentration was >16.7 mmol/L accompanied by diuresis and polydipsia, the rat was considered to be a diabetic [22–24]. The blood glucose concentration was determined after PBM once weekly (Fig. 2).

2.14. Wound establishment

Animals were intraperitoneally anesthetized with 10% chloral hydrate (Fuchen Chemical Reagents Co., Tianjin, China). After inducing deep anesthesia, a scalpel was used to make a 6 ×8 mm full-thickness skin wound on the dorsal side of the rat hind foot to simulate a mimic diabetic foot ulcer (mDFU) wound.

Biomedical Optics EXPRESS

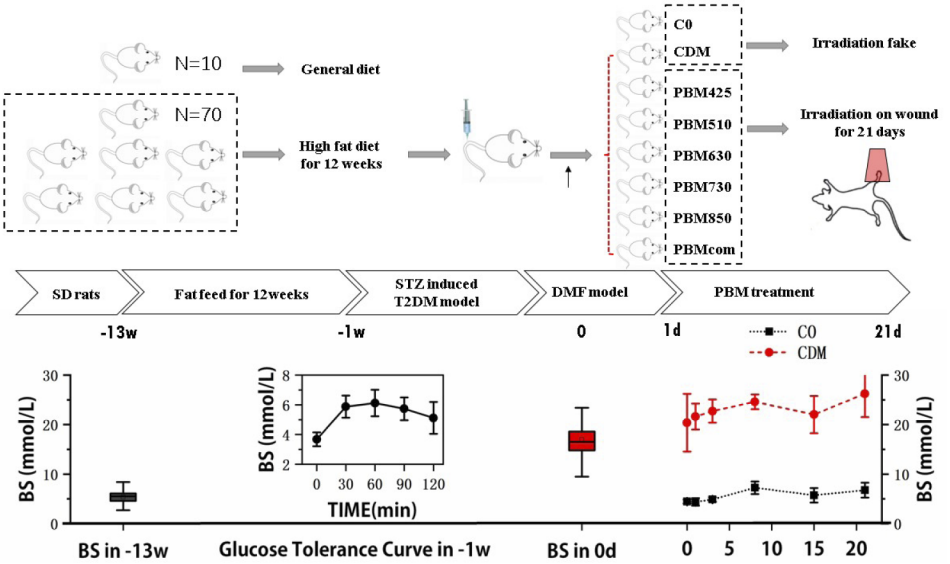

Fig. 2. Schematic diagram of in vivo experiments. SD rats were randomly divided into three groups: (1) healthy rats not submitted to a high-fat diet and not treated with PBM (C0, n = 10); (2) rats with type 2 diabetes mellitus without PBM treatment (CDM, n = 10); (3) rates with type 2 diabetes mellitus with various PBM therapies including PBM at 425 nm (n = 10), 510 nm (n = 10), 630 nm (n = 10), 730 nm (n = 10), 850 nm (n = 10), and PBM with multiple wavelength combinations (PBMcom, n = 10). Group C0 were fed a general diet. Group CDM and PBM groups were fed with a high-fat diet for 12 weeks and achieved impaired glucose tolerance. Then, a single tail vein injection of 30 mg/kg STZ was administered to induce diabetes. One week later (day 0), diabetes was diagnosed in rats with blood glucose of >16.7 mmol/L and a 6 × 8 mm full-thickness skin wound was made to establish the mimic DMF model. PBM was administered to right-sided DFUs 24 h after injury for 5 days a week. Blood glucose concentration was determined after PBM once weekly.

2.15. PBM therapy in vivo

Irradiation was performed with the set of LED devices shown in Fig. 1(e)–1(h). LED devices had a beam spot of 5 cm and power density of 10 mW/cm^2 at a distance of 2 cm. PBM was performed at 24 h after injury to the right mDFU for 5 days a week. Irradiation was applied in a continuous wave at a radiant exposure of 4 J/cm^2/day (Table 1c). Left mDFUs were sham-irradiated as a control.

2.16. PBMcom design strategy

Considering the proliferative effect of PBM at different wavelengths on four diabetic cell lines, we selected 425, 510, 630, 730, and 850 nm as the wavelengths in each 100 nm band for subsequent experiments. However, the role of PBM in treating monolayered cells can not represent organism. Different wavelength-compatible treatment strategies can be used in accordance with the required penetration depth in the clinic. The preliminary effect was acceleration of inflammatory cell infiltration in the early stage of healing (1–3 days) using 510 and 850 nm. After 3–7 days, it continued to promote vascular cell and fibroblast proliferation using 850 and 510 nm. At 7-11 days, fibroblasts and keratinocytes should still be promoted, Therefore, 510 and 630 nm were used. After 11–21 days, 425 nm was used mainly for keratinocytes. In this study, 730 nm light improved energy metabolism in HaCaT cells (Fig. 5(a)), and in previous studies [25,26], 730 nm light enhanced wound closure. Therefore, we also used 730 nm light during wound remodeling.

Biomedical Optics EXPRESS

2.17. Wound area measurement

The wound was imaged using a digital camera every 2 days for 21 consecutive days, beginning immediately after PBM. The digital camera was fixed on a special support above the animal experiment table to ensure a consistent shooting angle and distance. Lesions were analyzed using Image J software. The wound closure rate (%) was reached as Eq. (2):

$$Wound\ closure\ (\%) = \frac{S_{\text{wound area}} - S_{\text{wound area on Day 1}}}{S_{\text{wound area on Day 1}}} \tag{2}$$

2.18. Wound blood perfusion measurements

Wound blood perfusion was measured using a laser speckle imager (Moor FLPI; Moor Instruments Co., UK) in the first 7 days. Image processing and analysis employed Moor-FLPI software. The average blood flow perfusion value was automatically generated.

2.19. H&E and immunohistochemistry

On days 3 (n = 2), 7 (n = 2), and 15 (n = 6), rats were sacrificed and wound tissue was collected for H&E staining and immunohistochemistry. Specimens, including the original wound plus the surrounding normal tissue, were excised and fixed in 4% paraformaldehyde. Tissue slides were stained with H&E (Solarbio, Beijing, China) to measure defect size and Masson's trichrome stain to assess collagen synthesis. The collagen volume fraction (CVF) was calculated by ImageJ software in accordance with the staining intensity. Immunohistochemistry was used to assess proliferation (PCNA), angiogenesis (CD34), immune activation (CD11B), and MMP-9 expression. Sections were scanned (20× magnification) using a full-field digital slice imaging system (C13210-01; Hamamatsu, Japan). Immunoblots were quantitatively assessed using ImageJ software.

2.20. Scores for the contribution of PBM wavelengths to mDFU healing

The effects of PBM wavelengths on mDFU healing were evaluated and scored in the cell models and in the animal model. The biological effect that was beneficial to healing was counted as 1 point, and the biological effect that was harmful to healing was counted as −1 point. All PBM therapy groups were scored respectively and divided into two bands (400–600 nm and 600–900 nm), and scores were weighted in vitro and in vivo.

2.21. Statistical analysis

Data analysis employed SPSS 22.0. Results are presented as the mean ± standard error. Percentages represent group means. The D'Agostino and Pearson omnibus normality test was used to determine normality. The two-tailed unpaired t-test was used to analyze comparative data of two sets of normally distributed data. Comparisons of three groups or more than three groups of normally distributed data were analyzed using one-way analysis of variance, followed by the least significant difference multiple comparison test.

3. Results

3.1. Cell proliferation

Fibroblasts (WS1), endothelial cells (HUVECs), keratinocytes (HaCaT), and macrophages (U937) were used as targeted DFU cells. The four cell types were subjected to different concentrations of glucose for 3 days prior to PBM to simulate the high-glucose environment observed in diabetes mellitus. As shown in Fig. 3, high glucose treatment with 10 g/L glucose notably downregulated the viability of all four cell types. Thus, culture conditions with 10 g/L glucose were used (high-glucose model).

Biomedical Optics EXPRESS

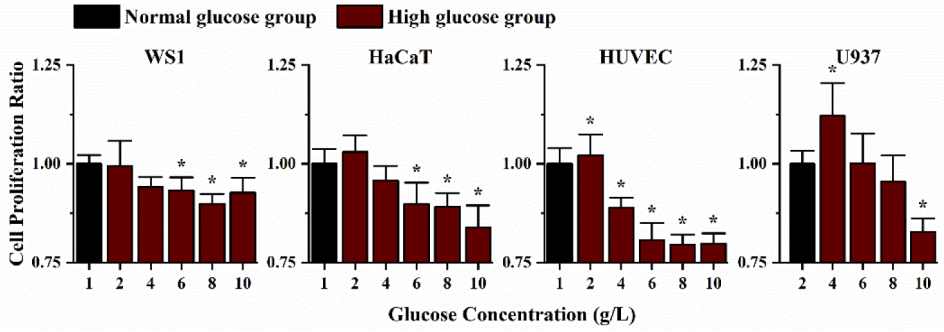

Fig. 3. Effects of high glucose on cell viability. The four cell lines were incubated in various concentrations of glucose for 3 days, following by MTT assays to assess cell viability. The inhibitory effects of high glucose on cell proliferation were sequenced as HUVECs > HACAT cells > U937 cells > WS1 cells. A concentration of 10 g/L glucose inhibited proliferation of all four cell types; thus, this concentration of glucose was used to simulate the high glucose conditions observed in diabetes mellitus in further experiments. *P < 0.05 vs. normal glucose group.

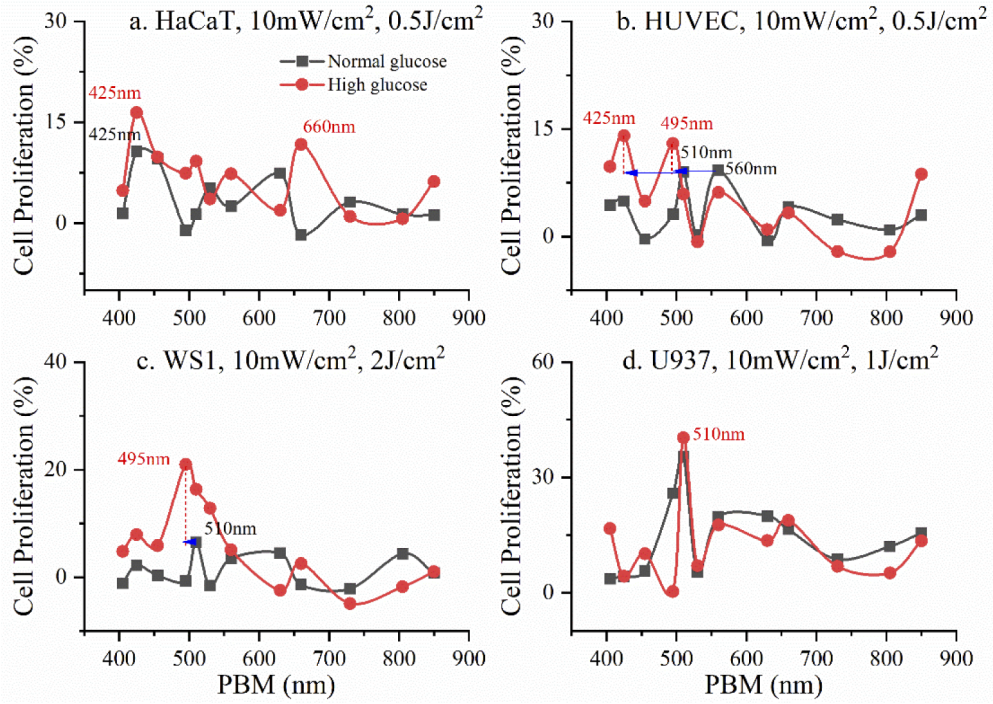

Fig. 4. Proliferation of HaCaT cells (a), HUVECs (b), WS1 cells (c), and U937 cells (d) induced by PBM therapy with a wide-spectrum range of LEDs (400–900 nm) under normal and high-glucose culture conditions. HaCaT: human immortalized keratinocytes; HUVECs: human umbilical vein endothelial cells; WS1: human skin fibroblasts; U937: human monocyte-like cells.

Biomedical Optics EXPRESS

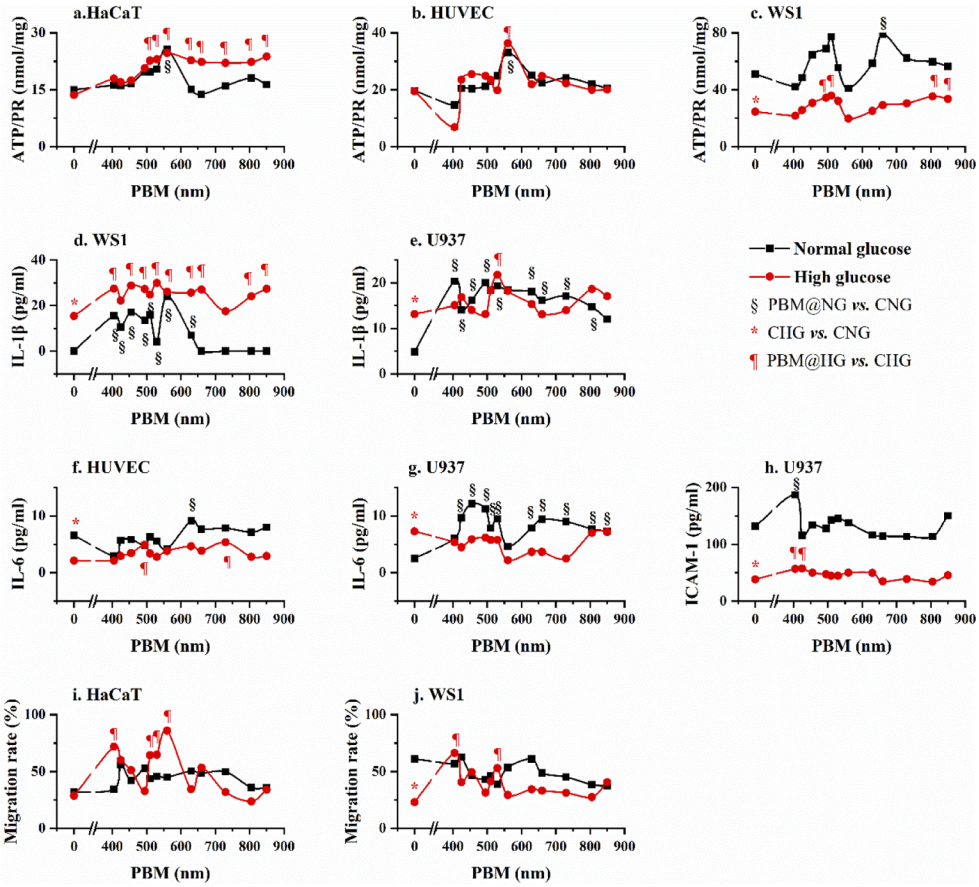

Fig. 5. Adenosine triphosphate production (a–c), secretion (d–h), and migration (i–j) of cell models induced by photo-biomodulation (PBM). *P < 0.05, control group in normal glucose (CNG) vs. control group in high glucose (CHG). §P < 0.05, PBM in normal glucose (PBM@NG) vs. CNG. ¶P < 0.05, PBM in high glucose (PBM@HG) vs. CHG.

Cell proliferation induced by PBM at different wavelengths from visible to near-infrared (405, 425, 455, 495, 510, 530, 560, 630, 660, 730, 805, and 850 nm) was measured at a series of energy settings (0.5, 1, 2, 4, 6, 8, and 10 J/cm^2) and power densities (10 and 40 mW/cm^2) using the MTT assay. Dose–effect curves are shown in Figs. S1–4. A power density of 10 mW/cm^2 presented better effects compared with 40 mW/cm^2, and the energy range of 0.5–2 J/cm^2 showed peak effects on cell proliferation. The PBM wavelength effects on the targeted cells at 10 mW/cm^2 and 0.5–2 J/cm^2 (peak effects) are shown in Fig. 4.

We found that PBM had several proliferation-promoting peaks in each of the four targeted cell types in the normal (black curve) and diabetic (red curve) models. The peaks in the diabetic model were bimodal, and were named bimodal effects of the PBM wavelength spectrum. PBM showed obvious bimodal effects at 425 nm and 660 nm in diabetic HaCaT cells (Fig. 4(a)). In three other diabetic cell types, the peak effects in the red–infrared band were weaker compared with the green–blue band (425 nm in HUVECs, 495 nm in WS1 cells, and 510 nm in U937 cells). Another effect of the PBM wavelength spectrum was a shift to the short wavelength region (blue shift). The wavelength blue shift was most pronounced in HUVECs (425 nm and 495 nm in the diabetic model *vs.* 510 nm and 560 nm in the normal model [blue arrow, Fig. 4(b)]).

Biomedical Optics EXPRESS

3.2. Adenosine triphosphate (ATP) production/secretion and cell migration

ATP production is a major indicator of cellular activity and is often impaired under diabetic conditions. ATP production in WS1 cells decreased significantly compared with the normal model ($P < 0.001$). PBM with green light (495 and 510 nm) and near-infrared light (805 and 850 nm) increased the impairment in ATP production (Fig. 5(c)). A long band of light (510–850 nm) increased ATP production in HaCaT cells in the diabetic model (Fig. 5(a)). Irradiation with 560 nm significantly increased ATP production in HUVECs in both normal and diabetic models (Fig. 5(b)).

The concentrations of IL-1β, IL-6, and ICAM-1 were measured to evaluate the secretory function of targeted cells (Fig. 5(d)–5(h)). PBM significantly increased the IL-1β concentration in WS1 cells in the diabetic model at almost all wavelengths, except 425 and 730 nm (Fig. 5(d)), while the baseline IL-1β concentration in the diabetic model was higher compared with the normal model. A similar increment occurred in diabetic U937 cells under irradiation at 530 nm (Fig. 5(e)). Compared with IL-1β, IL-6 was less responsive to PBM in the diabetic model, while a strong response was observed in the normal model (Fig. 5(e) and 5(g)). Irradiation at 405 and 425 nm improved the impaired secretion of ICAM-1 in diabetic U937 cells (Fig. 5(h).

PBM showed an obvious blue–green band effect on target cell migration. Light at 405, 510, 530, and 560 nm significantly enhanced migration of diabetic HaCaT cells ($P = 0.012$, 0.049, 0.032, 0.004, respectively; Fig. 5(i)), and light at 405 and 530 nm improved migration of WS1 cells ($P = 0.001$, 0.045, respectively; Fig. 5(j)).

In general, bimodal effects of PBM wavelengths were obvious at the cellular level, and the blue–green band effect was stronger compared with the infrared band effect.

3.3. Wound healing in the mDFU animal model

To verify the bimodal effect of PBM, wavelengths of 425, 510, 630, 730, and 850 nm were used in the rat model of T2DM. A combination of PBM (PBMcom, green–blue band and red–infrared band; Table 1c) was also designed. A blood glucose concentration >16.7 mmol/L was used to evaluate the type 2 diabetes mellitus model. Full-thickness skin wounds on both feet were made to simulate DFUs. The wounds on the right foot were irradiated (irradiated foot), while the left foot (non-irradiated foot) was used as a self-control and verification model of the systemic effects of PBM. PBM irradiation did not affect blood glucose concentration in rats (Fig. 2).

The wound healing process in T2DM rats lagged compared with that of healthy rats (Fig. 6(a)–6(d)). At days 5 and 10, the wound size of healthy rats was significantly smaller compared with the wound size of rats with type 2 diabetes mellitus ($P = 0.001$ and $P < 0.001$, respectively; Fig. 6(c)). The time of wound healing in T2DM rats was 5 days longer than healthy rats ($P < 0.001$; Fig. 6(d)).

PBM shortened the healing process at all wavelengths (Fig. 6(e)–6(h)). At day 5, the wound sizes with PBM at 850 nm and PBMcom were significantly smaller than CDM ($P = 0.008$ and $P = 0.012$, respectively). At day 10, the wounds with PBM at 425 nm, PBM at 630 nm, and PBMcom were significantly smaller compared with CDM ($P = 0.045$, 0.039, and 0.004, respectively; Fig. 6(e)). For the irradiated foot (Fig. 6(h)), irradiated foot), PBMcom and red–infrared light (PBM at 630 nm, PBM at 730 nm, and PBM at 850 nm) had obvious positive effects on wound healing, as did PBM at 425 nm. PBMcom demonstrated the fastest wound healing speed (12 days). Notably, PBM at 510 nm demonstrated less of an improvement in wound healing, and the wounds became inflamed (swollen and exuded, as shown in Fig. 6(f)).

Interestingly, the healing speed of the non-irradiated foot with PBM at 630 nm, 730 nm, 850 nm, and PBMcom was significantly faster compared with the control group (Fig. 6(h)), non-irradiated foot). At day 5, the wounds with PBM at 630 nm, 730 nm, 850 nm, and PBMcom were significantly smaller compared with CDM (Fig. 6(e), right image). This implies that treatment with PBM increases immunity in rats.

Biomedical Optics EXPRESS

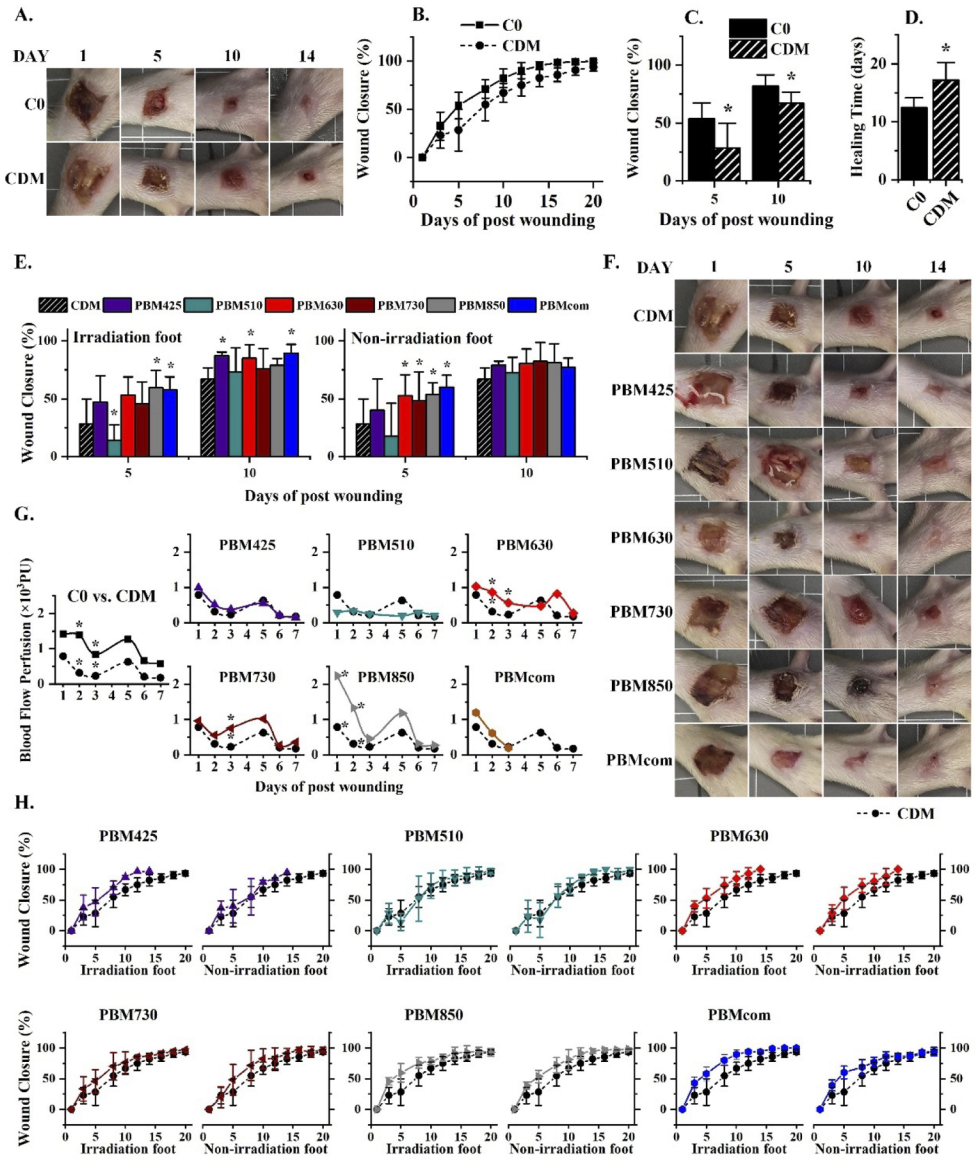

Fig. 6. PBM wound healing of mDFUs in T2DM rats. (a–d) Natural process of wound healing in healthy rats (C0) and T2DM rats (CDM). (a) Images of wound healing. (b) Curves of percentage wound healing. (c) Significant time points in wound healing in C0 compared with CDM. d. Healing time in C0 compared with CDM. (e–h) Healing process after PBM in CDM. (e) Wound healing percentage at significant time points (5 and 10 days) on the right foot (irradiated foot) and left foot (non-irradiated foot). (f) Images of wound healing after PBM (right foot). (g) Wound blood flow perfusion detected by laser speckle against time after PBM (irradiated foot). (h) Curves of percentage wound healing of the irradiated foot and non-irradiated foot. Block curves represent the results of CDM. Color curves represent the results of PBM. $*P < 0.05$.

Biomedical Optics EXPRESS

Wound blood perfusion was measured using a laser speckle imager to determine the efficacy of PBM (Fig. 6(g)). Blood perfusion in rats with type 2 diabetes mellitus (CDM) was significantly lower compared with healthy rats (C0) ($P = 0.001$ and 0.002 at days 2 and 3, respectively). PBM (630, 730, and 850 nm) improved wound blood perfusion, and PBM at 850 nm had the most positive effect.

3.4. Histological pathology of wound healing

Wounds were stained with H&E to observe epithelial growth. Epithelial growth of the CDM group was significantly decreased compared with that of the C0 group on day 3 ($P < 0.001$), whereas PBM at 630 nm significantly promoted slower epithelial growth in the CDM group ($P < 0.001$). However, PBM using green light (510 nm) inhibited epithelial growth on day 3 ($P = 0.001$). The reason might be that PBM510 promotes inflammation, which leads to excessive local inflammation and hinders epithelial growth. During wound healing, the epithelium completely covered the wound after PBM at 425 and 730 nm, and PBMcom on day 7, and in all groups on day 15 (Fig. 7(a)).

Tissue regeneration was indicated by PCNA to assess PBM. During the whole healing process (days 3, 7, and 15), wound tissue regeneration in the CDM group was significantly lower than that in the C0 group ($P < 0.001$). PBM promoted wound tissue regeneration during the healing process. However, the performance of different PBM in the process of wound healing was different. In terms of PCNA-positive cell counts, PBMcom reached the highest on day 3 (2688/mm^2, $P < 0.001$). Pbm425 reached the highest on day 7 (5688/mm^2, $P = 0.013$). PBM510 and PBM850 reached the highest on day 15 (5948/mm2, $P < 0.001$ and 4512.82mm2, $P = 0.002$, respectively). PBM730 had a good effect on promoting tissue proliferation on both days 3 and 7 (3179/mm^2, P < 0.001, 5912/mm^2, $P = 0.004$) (Figs. 7(b) and S5).

Angiogenesis was detected by CD34 staining. We observed a significant delay in diabetic wound angiogenesis in CDM rats compared with that in control rats. PBM730 and PBMcom showed significant promotion of the delay in angiogenesis on days 3 and 7 ($P < 0.001$). However, PBM510 showed the opposite effect of this delay in the early stage until supplementary angiogenesis was achieved on day 15, which was consistent with the results of PBM510 activating inflammation (Figs. 7(c) and S6).

Inflammatory cell infiltration was detected by CD11B staining. The mDFU model exhibited a slow and lasting inflammatory response similar to that in the clinic. PBM showed bidirectional regulation of inflammation, which promoted the inflammatory response in the early stage (e.g., PBM425, PBM630, and PBM730 on day 3) and inhibited the inflammatory response in the late stage (PBM at all wavelengths on day 15). PBM510 was in a state of stimulating the inflammatory response from beginning to end. This was consistent with the results of several indicators (Figs. 7(d) and S7).

Wound healing is closely related to the dynamic balance of the extracellular matrix. MMP-9 is a major protease involved in degradation of the extracellular matrix [27]. Throughout the healing process, MMP-9 was highly expressed in mDFU wounds. All PBM groups had significantly decreased expression of MMP-9 due to diabetes mellitus during the wound healing process (days 3, 7, and 15, $P < 0.05$) with the exception of PBM at 850 nm on day 7 (Fig. 7(e) and S8).

Collagen remodeling was visualized by Masson's trichrome staining (Figs. 7(f) and S9). Collagen deposition was quantified by the collagen volume fraction (CVF). As observed previously, hyperglycemia inhibited collagen deposition and the CVF in DUF model rats was significantly lower than that in the healthy control group. PBM treatment significantly improved collagen deposition during the whole wound healing process at all wavelengths (Fig. 7(f)).

Biomedical Optics EXPRESS

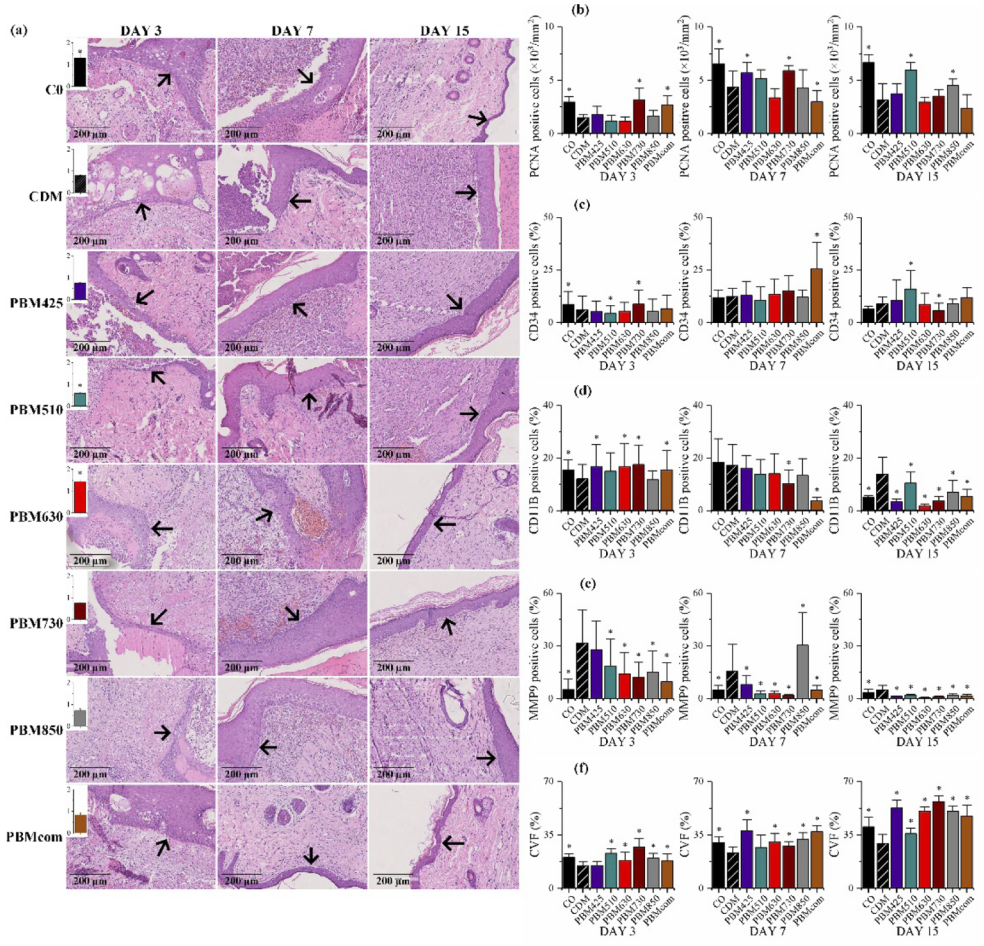

Fig. 7. Pathology of wound healing. (a) Wounds stained by hematoxylin and eosin (H&E). Arrows show the epithelial tongue position. PBM at 630 nm significantly promoted Mdfu epithelial growth on day 3. On day 7, the epithelium had completely covered the wound in some PBM groups (PBM425, PBM730, and PBMcom). On day 15, it had completed in all groups. (b) Quantification of PCNA (index of tissue regeneration). Partial wavelength PBM significantly promoted the proliferation of wound cells. For example, PCNA expression in PBM730 and PBMcom groups was increased on days 3 and 7. (c) Quantification of CD34 (index of angiogenesis). PBM730 promoted neovascularization on day 3 and PBMcom promoted angiogenesis on day 7. (d). Quantification of CD11B (index of inflammatory infiltration). PBM reversed slow and long-lasting mDFU inflammation. (e) Quantification of matrix metalloproteinase-9 (MMP-9). PBM decreased MMP-9 expression, except for PBM850 on day 7. (f) Quantification of collagen deposition. The collagen deposition ratio was calculated by the collagen volume fraction (CVF). All PBM treatments significantly improved collagen deposition. $^*P < 0.05$ vs. CDM (T2DM control group).

Biomedical Optics EXPRESS

4. Discussion

The wound healing process is divided into three different but overlapping stages: inflammation, proliferation, and remodeling [28]. In this process, cells (inflammatory cells, myofibroblasts, and endothelial cells) are recruited to the wound bed and interact with resident cells to replace damaged or lost tissue and restore the skin integrity [19]. To simulate this complex wound healing phenomenon, we examined the responses of four related cell types subjected to PBM in a high-glucose environment and performed spectral effect analysis of PBM in a DFU animal model. The results showed that PBM effectively promoted DFU wound healing and had a bimodal effect in accordance with the wavelength spectra: blue–green and red–infrared band effects. PBMcom exerted this bimodal effect and had a positive effect on DFU healing.

In accordance with the first law of photochemistry, a photochemical reaction can only occur after a photon is absorbed by a photoreceptor or chromophore [29]. The absorption of monochromatic visible light or NIR light photons by endogenous chromophores is considered to be the basis for the PBM function at the cellular level [17]. The different molecular structures of chromophores selectively absorb light and reflect light of different wavelengths that impart a specific color to its constituent compounds [13]. Examples of such chromophores include hemoglobin, CCO, myoglobin, flavins, flavoproteins, porphyrins, tryptophan, chlorophyll (plants), the Soret band of heme groups, cryptochromes, light-gated ion channels, and opsins [17,30].

In animal models and humans, red–near-infrared PBM has shown benefits for osteoarthritis, pain control [31], management of adverse reactions to chemotherapy [32], and wound healing [33]. The basic mechanisms of red–near-infrared PBM have been postulated to involve mitochondrial cytochrome c oxidase (COX) that is activated by preferentially absorbing red light. [8] Activated COX increases ATP, cyclic adenosine monophosphate (cAMP), nitric oxide, the mitochondrial membrane potential, and calcium ion concentrations [8,34]. ATP and cAMP participate in the cAMP-dependent protein kinase A signaling pathway mediated by G protein-coupled receptors to phosphorylate target proteins and regulate cell responses [34]. Additionally, the intracellular redox state shifts after PBM and after application of electronic device-generated light [35,36].

The possible mechanism of green–blue light PBM remains unclear. Recently, Castellano-Pellicena et al. found that blue light PBM accelerates wound closure with an *Opsin 3* expression increase and keratinocyte metabolic activity enhancement [37]. Additionally, Yoshida et al. [36] found that blue light irradiation consumes intracellular glutathione, increases the production of reactive oxygen species, induces oxidative stress, and enhances lipid peroxidation. All of these may be potential mechanisms of blue light irradiation in promoting wound closure.

Although a variety of photoreceptors are present in cells and tissues, absorption of light can be divided into a green–blue band and a red–infrared band. DFU healing is not a simple cell proliferation process. There are many different types of cells involved and interactions with each other. We did not attempt to identify the photoreceptors involved in DFU healing; instead, we evaluated and scored the effects of the two PBM bands on the treatment of DFUs (Table S1). In the single-layer cell system, without considering light penetration depth, an evaluation of the four cell lines in DFU wound healing showed that the score of the green–blue band (400–600 nm) was higher compared with the red–infrared band (600–900 nm). However, in the thickness DFU tissue in vivo, which affected the propagation of light in the tissue, the score of the red–infrared band (630, 730, and 850 nm) was much higher compared with the green–blue band (425 and 510 nm). The two-band combination strategy of PBM scored better than the red–infrared band alone. In PBM therapy, two major parameters need to be considered, namely the wavelength of light absorbed by the photoreceptor and the effective penetration depth of light in the tissue [14]. Most previous studies of PBM have used red and NIR light (λ 600–1100 nm). This is because, in this light waveband, the effective penetration depth of light in the tissue reaches the maximum, which is from approximately 650 to 1200 nm [14,38]. However, we believe that the PBMcom

Biomedical Optics EXPRESS

strategy activates more photoreceptors at different depths of tissue, improving the efficacy of PBM.

In our in vitro experiment, we used MTT assays for high-throughput screening of optical parameters. The results depend on the number of viable cells and their metabolic activity, and not a specific marker that reflects cell proliferation [39]. However, regardless of cell promotion or viable cell metabolism, PBM had a positive effect on wound-healing cells in vitro. The screened optical parameters also showed a good healing effect in the in vivo experiment, except for 510 nm. Therefore, the actual effect of PBM in the clinic might be different from that of PBM on monolayered cells in culture.

Although the mechanism of delayed wound healing in diabetic patients has not been fully clarified, all stages of the healing process are disrupted, including impaired proliferation [40–42], delayed neovascularization [43,44], abnormal inflammation, and reduced collagen deposition [45]. Overall, PBM in this study had a positive effect on DFU healing-related indicators. However, the influence of PBM at various wavelengths on the indicators was different at each time point. For example, in the early and middle stages of wound healing, PBM630 was better than PBM730 in terms of the cell proliferation indicator PCNA, whereas in the late stage of wound healing, PBM730 was better than PBM630. This was different from our expectation that a certain wavelength would perform well for various indicators. This might be because different tissues and cells have different targets for specific light wavelengths. In vitro, the proliferation of the four cell lines responded differently to different wavelengths and the healing performance in vivo would be more complex. The wound response to PBM was related to the penetration depth and photoreceptor expression in the tissue. Additionally, PBM accelerates the healing of non-irradiated wounds. PBM has a significant regulatory effect on the immune functions of diabetic rats, and there is a systemic effect of LED phototherapy [46]. PBM is likely to have a systemic effect by activating inflammatory cells or immune cells in non-adjacent tissues. Different wavelengths of PBM might have different effects in the various stages of healing. Therefore, PBM with multiple wavelength combinations may compensate for the deficiency of monochromatic light similarly to our in vitro experiments. Notably, this study showed that PBM510 stimulated an inflammatory response and led to excessive inflammation during the whole process, which should be resolved in the PBMcom strategy. There may be more reasonable PBMcom strategy in the future, which require further study. Overall, this study provides the theoretical basis for PBM in clinical treatment of DFU.

5. Conclusion

In this study, we detected 12 wavelengths (400–900 nm) that induced PBM in DFUs in cell and animal models. At the single-layer cell level, the green–blue band (400–600 nm) had better wound-healing effects compared with the red–infrared band (600–900 nm). Inversely, at the organism level, the red–infrared band had better wound-healing effects compared with the green–blue band. In addition, a combination of the green–blue band and the red–infrared band presented a better effect compared with the two bands alone. In previous studies, the depth of light penetration in tissues was overemphasized and the diversity of light receptors in tissues was ignored; thus, red light-mediated PBM was generally considered the best treatment strategy. However, the results of this study suggest that a PBM strategy that combines blue–green light and red–infrared light is the best treatment strategy for DFUs and other open wounds.

Funding. National Key Research and Development Program of China (2017YFB0403804).

Acknowledgments. We thank Dr. Emily Woodhouse and Mitchell Arico from Liwen Bianji (Edanz) for editing the language of a draft of this manuscript.

Disclosures. The authors declare that there are no conflicts of interest related to this article

Biomedical Optics EXPRESS

Data availability. Data underlying the results presented in this paper are not publicly available at this time but may be obtained from the authors upon reasonable request.

Supplemental document. See Supplement 1 for supporting content.

References

1. G. S. Schultz, R. G. Sibbald, V. Falanga, E. A. Ayello, C. Dowsett, K. Harding, M. Romanelli, M. C. Stacey, L. Teot, and W. Vanscheidt, "Wound bed preparation: a systematic approach to wound management," Wound Repair Regen **11**(s1), S1–S28 (2003).
2. J. L. Richard, A. Sotto, and J. P. Lavigne, "New insights in diabetic foot infection," WJD **2**(2), 24–32 (2011).
3. P. K. Moulik, R. Mtonga, and G. V. Gill, "Amputation and mortality in new-onset diabetic foot ulcers stratified by etiology," Diabetes Care **26**(2), 491–494 (2003).
4. L. D. Woodruff, J. M. Bounkeo, W. M. Brannon, K. S. Dawes, C. D. Barham, D. L. Waddell, and C. S. Enwemeka, "The efficacy of laser therapy in wound repair: a meta-analysis of the literature," Photomed. Laser Surg. **22**(3), 241–247 (2004).
5. M. S. Dawood and S. D. Salman, "Low level diode laser accelerates wound healing," Lasers Med. Sci. **28**(3), 941–945 (2013).
6. P. C. Silveira, L. A. Silva, T. P. Freitas, A. Latini, and R. A. Pinho, "Effects of low-power laser irradiation (LPLI) at different wavelengths and doses on oxidative stress and fibrogenesis parameters in an animal model of wound healing," Lasers Med. Sci. **26**(1), 125–131 (2011).
7. Z. Mao, J. H. Wu, T. Dong, and M. X. Wu, "Additive enhancement of wound healing in diabetic mice by low level light and topical CoQ10," Sci. Rep. **6**(1), 20084 (2016).
8. L. F. de Freitas and M. R. Hamblin, "Proposed mechanisms of photobiomodulation or low-level light therapy," IEEE J. Sel. Top. Quantum Electron. **22**(3), 348–364 (2016).
9. T. Ando, W. Xuan, T. Xu, T. Dai, S. K. Sharma, G. B. Kharkwal, Y. Y. Huang, Q. Wu, M. J. Whalen, S. Sato, M. Obara, and M. R. Hamblin, "Comparison of therapeutic effects between pulsed and continuous wave 810-nm wavelength laser irradiation for traumatic brain injury in mice," PloS one **6**(10), e26212 (2011).
10. D. Gigo-Benato, S. Geuna, A. de Castro Rodrigues, P. Tos, M. Fornaro, E. Boux, B. Battiston, and M. G. Giacobini-Robecchi, "Low-power laser biostimulation enhances nerve repair after end-to-side neurorrhaphy: a double-blind randomized study in the rat median nerve model," Lasers Med. Sci. **19**(1), 57–65 (2004).
11. T. Y. Chung, P. V. Peplow, and G. D. Baxter, "Laser photobiostimulation of wound healing: defining a dose response for splinted wounds in diabetic mice," Lasers Surg. Med. **42**(9), 816–824 (2010).
12. A. Schindl, M. Schindl, H. Pernerstorfer-Schon, K. Kerschan, R. Knobler, and L. Schindl, "Diabetic neuropathic foot ulcer: successful treatment by low-intensity laser therapy," Dermatology (Basel, Switz.) **198**(3), 314–316 (1999).
13. Y. Y. Huang, A. C. Chen, J. D. Carroll, and M. R. Hamblin, "Biphasic dose response in low level light therapy," Dose-Response **7**(4), 358–383 (2009).
14. Y. Y. Huang, S. K. Sharma, J. Carroll, and M. R. Hamblin, "Biphasic dose response in low level light therapy - an update," Dose-Response **9**(4), 602–618 (2011).
15. J. J. Anders, R. J. Lanzafame, and P. R. Arany, "Low-level light/laser therapy versus photobiomodulation therapy," Photomed. Laser Surg. **33**(4), 183–184 (2015).
16. T. Karu, "Photobiology of low-power laser effects," Health Phys. **56**(5), 691–704 (1989).
17. M. R. Hamblin, "Mechanisms and mitochondrial redox signaling in photobiomodulation," Photochem. Photobiol. **94**(2), 199–212 (2018).
18. Y. Wang, Y. Y. Huang, Y. Wang, P. Lyu, and M. R. Hamblin, "Photobiomodulation (blue and green light) encourages osteoblastic-differentiation of human adipose-derived stem cells: role of intracellular calcium and light-gated ion channels," Sci. Rep. **6**(1), 33719 (2016).
19. J. M. Reinke and H. Sorg, "Wound repair and regeneration," Eur. Surg. Res. **49**(1), 35–43 (2012).
20. P. Martin, "Wound healing–aiming for perfect skin regeneration," *Science* (New York, N.Y.) 276, 75–81 (1997).
21. J. Li, J. Chen, and R. Kirsner, "Pathophysiology of acute wound healing," Clin. Dermatol. **25**(1), 9–18 (2007).
22. G. Pyun do, H. J. Choi, H. S. Yoon, T. Thambi, and D. S. Lee, "Polyurethane foam containing rhEGF as a dressing material for healing diabetic wounds: synthesis, characterization, in vitro and in vivo studies," Colloids Surf., B **135**, 699–706 (2015).
23. A. B. Gaikwad, B. Viswanad, and P. Ramarao, "PPAR gamma agonists partially restores hyperglycemia induced aggravation of vascular dysfunction to angiotensin II in thoracic aorta isolated from rats with insulin resistance," Pharmacol. Res. **55**(5), 400–407 (2007).
24. C. O. Yu, K. S. Leung, J. L. Jiang, T. B. Wang, S. K. Chow, and W. H. Cheung, "Low-magnitude high-frequency vibration accelerated the foot wound healing of n5-streptozotocin-induced diabetic rats by enhancing glucose transporter 4 and blood microcirculation," Sci. Rep. **7**(1), 11631 (2017).
25. R. Ankri, R. Lubart, and H. Taitelbaum, "Estimation of the optimal wavelengths for laser-induced wound healing," Lasers Surg. Med. **42**(8), 760–764 (2010).
26. A. L. Pinheiro, G. C. Meireles, C. M. Carvalho, L. M. Ramalho, and J. N. dos Santos, "Biomodulative effects of visible and IR laser light on the healing of cutaneous wounds of nourished and undernourished Wistar rats," Photomed. Laser Surg. **27**(6), 947–957 (2009).

Biomedical Optics EXPRESS

27. M. Xue, N. T. Le, and C. J. Jackson, "Targeting matrix metalloproteases to improve cutaneous wound healing," Expert Opin. Ther. Targets **10**(1), 143–155 (2006).
28. G. C. Gurtner, S. Werner, Y. Barrandon, and M. T. Longaker, "Wound repair and regeneration," Nature **453**(7193), 314–321 (2008).
29. J. C. Sutherland, "Biological effects of polychromatic light," Photochem. Photobiol. **76**(2), 164–170 (2002).
30. T. Karu, "Primary and secondary mechanisms of action of visible to near-IR radiation on cells," J. Photochem. Photobiol., B **49**(1), 1–17 (1999).
31. R. Dima, V. Tieppo Francio, C. Towery, and S. Davani, "Review of literature on low-level laser therapy benefits for nonpharmacological pain control in chronic pain and osteoarthritis," Alternative therapies in health and medicine **24**(5), 8–10 (2018).
32. J. A. Zecha, J. E. Raber-Durlacher, R. G. Nair, J. B. Epstein, S. T. Sonis, S. Elad, M. R. Hamblin, A. Barasch, C. A. Migliorati, D. M. Milstein, M. T. Genot, L. Lansaat, R. van der Brink, J. Arnabat-Dominguez, L. van der Molen, I. Jacobi, J. van Diessen, J. de Lange, L. E. Smeele, M. M. Schubert, and R. J. Bensadoun, "Low level laser therapy/photobiomodulation in the management of side effects of chemoradiation therapy in head and neck cancer: part 1: mechanisms of action, dosimetric, and safety considerations," Support Care Cancer **24**(6), 2781–2792 (2016).
33. P. Avci, A. Gupta, M. Sadasivam, D. Vecchio, Z. Pam, N. Pam, and M. R. Hamblin, "Low-level laser (light) therapy (LLLT) in skin: stimulating, healing, restoring," Semin Cutan Med Surg **32**(1), 41–52 (2013).
34. X. Gao and D. Xing, "Molecular mechanisms of cell proliferation induced by low power laser irradiation," J. Biomed. Sci. **16**(1), 4 (2009).
35. E. Austin, A. Huang, T. Adar, E. Wang, and J. Jagdeo, "Electronic device generated light increases reactive oxygen species in human fibroblasts," Lasers Surg. Med. **50**(6), 689 (2018).
36. A. Yoshida, Y. Shiotsu-Ogura, S. Wada-Takahashi, S. S. Takahashi, T. Toyama, and F. Yoshino, "Blue light irradiation-induced oxidative stress in vivo via ROS generation in rat gingival tissue," J. Photochem. Photobiol., B **151**, 48–53 (2015).
37. I. Castellano-Pellicena, N. E. Uzunbajakava, C. Mignon, B. Raafs, V. A. Botchkarev, and M. J. Thornton, "Does blue light restore human epidermal barrier function via activation of Opsin during cutaneous wound healing?" Lasers Surg. Med. **51**(4), 370–382 (2019).
38. T. I. Karu and N. I. Afanas'eva, "Cytochrome c oxidase as the primary photoacceptor upon laser exposure of cultured cells to visible and near IR-range light," Doklady Akademii nauk **342**(4), 693–695 (1995).
39. T. L. Riss, R. A. Moravec, A. L. Niles, S. Duellman, H. A. Benink, T. J. Worzella, and L. Minor, "Cell Viability Assays," in *Assay Guidance Manual*, S. Markossian, A. Grossman, K. Brimacombe, M. Arkin, D. Auld, C. P. Austin, J. Baell, T. D. Y. Chung, N. P. Coussens, J. L. Dahlin, V. Devanarayan, T. L. Foley, M. Glicksman, M. D. Hall, J. V. Haas, S. R. J. Hoare, J. Inglese, P. W. Iversen, S. C. Kales, M. Lal-Nag, Z. Li, J. McGee, O. McManus, T. Riss, P. Saradjian, G. S. Sittampalam, M. Tarselli, O. J. Trask Jr., Y. Wang, J. R. Weidner, M. J. Wildey, K. Wilson, M. Xia, and X. Xu, eds. (Eli Lilly & Company and the National Center for Advancing Translational Sciences, 2004).
40. J. Wysocki, B. Wierusz-Wysocka, A. Wykretowicz, and H. Wysocki, "The influence of thymus extracts on the chemotaxis of polymorphonuclear neutrophils (PMN) from patients with insulin-dependent diabetes mellitus (IDD)," Thymus **20**(1), 63–67 (1992).
41. C. O. Yu, K. S. Leung, K. P. Fung, F. F. Lam, E. S. Ng, K. M. Lau, S. K. Chow, and W. H. Cheung, "The characterization of a full-thickness excision open foot wound model in n5-streptozotocin (STZ)-induced type 2 diabetic rats that mimics diabetic foot ulcer in terms of reduced blood circulation, higher C-reactive protein, elevated inflammation, and reduced cell proliferation," Exp. Anim. **66**(3), 259–269 (2017).
42. A. J. Boulton, "End-stage complications of diabetic neuropathy: foot ulceration," The Canadian J. Neurological Sci. **21**(S4), S18–22; discussion S23-15 (1994).
43. G. Zhou, X. Han, Z. Wu, Q. Shi, and X. Bao, "Rosiglitazone accelerates wound healing by improving endothelial precursor cell function and angiogenesis in db/db mice," PeerJ **7**, e7815 (2019).
44. G. Han and R. Ceilley, "Chronic wound healing: a review of current management and treatments," Adv. Ther. **34**(3), 599–610 (2017).
45. W. H. Goodson, 3rd and T. K. Hunt, "Wound healing and the diabetic patient," Surgery, Gynecology & Obstetrics **149**, 600–608 (1979).
46. G. Y. Lee and W. S. Kim, "The systemic effect of 830-nm LED phototherapy on the wound healing of burn injuries: A controlled study in mouse and rat models," J. Cosmetic and Laser Therapy **14**(2), 107–110 (2012).